NiFe-layered double hydroxide arrays for oxygen evolution reaction in fresh water and seawater

Guofa Dong [a, f], Fengyan Xie [a, f], Fangxia Kou [a], Tingting Chen [a], Fengyun Wang [b], Yingwu Zhou [a], Kechen Wu [a], Shaowu Du [a, **], Ming Fang [c, ***], Johnny C. Ho [d, e, *]

[a] *Fujian Key Laboratory of Functional Marine Sensing Materials, Minjiang University, Fuzhou 350108, China*
[b] *College of Physics and State Key Laboratory of Bio Fibers and Eco Textiles, Qingdao University, Qingdao 266071, China*
[c] *Shenzhen Key Laboratory of Special Functional Materials, Guangdong Research Center for Interfacial Engineering of Functional Materials, College of Materials Science and Engineering, Shenzhen University, Shenzhen 518060, China*
[d] *Department of Materials Science and Engineering and State Key Laboratory of Terahertz and Millimeter Waves, City University of Hong Kong, Kowloon 999077, Hong Kong Special Administrative Region*
[e] *Key Laboratory of Advanced Materials Processing & Mold (Zhengzhou University), Ministry of Education, Zhengzhou 450002, China*

ARTICLE INFO

ABSTRACT

The development of active, durable, and cost-effective electrocatalysts for the oxygen evolution reaction (OER) is crucial for viable hydrogen production from water by electrolysis. In this work, we report a mild, atmospheric pressure-based chemical method for the synthesis of NiFe-containing layered double hydroxide (LDH) nanosheet arrays on a carbon fiber cloth (CC). The obtained NiFe-LDH/CC composites with various Ni/Fe ratios show good performance for OER in alkaline aqueous solutions. Among them, the sample with a Ni/Fe ratio of 6:4 exhibits the best OER activity with overpotential values of only 226 mV in water and 238 mV in seawater at a current density of 10 mA cm^{-2}, which are much lower than those of the benchmarking RuO$_2$ catalyst. The catalytic activity can be maintained for at least 450 h for OER in fresh water and 165 h in seawater at a current density of 100 mA cm^{-2}.

© 2021 Elsevier Ltd. All rights reserved.

1. Introduction

Hydrogen is widely recognized as an ideal future energy carrier because of its zero pollution emission and high energy density [1–5]. It is therefore urgent to explore methods for producing hydrogen cost-effectively and environmentally friendly. Water electrolysis is particularly suitable for this purpose as it can be powered by renewable energy sources [6–9]. Water electrolysis proceeds through two half-reactions, including the cathodic hydrogen evolution reaction (HER) and anodic oxygen evolution reaction (OER) [10]. Although HER is a two-electron transfer reaction, OER involves a four-electron transfer process, which makes OER kinetically more sluggish [11]. This way, the overpotential associated with OER is always higher than that of HER. In this

regard, the development of low-cost, active, and robust OER electrocatalysts is intriguingly important for enabling water electrolysis for practical hydrogen production [12].

In general, the state-of-the-art OER electrocatalysts for commercial use are mostly composed of noble metal compounds, such as RuO$_2$ and IrO$_2$ [13]. These noble metal-based catalysts are not only very expensive but also scarce on earth. Extensive efforts have then been devoted to exploring non-noble alternative OER catalysts with high activity and good stability by using earth-abundant elements. Recently, various nickel-iron-based catalysts, including their alloys [14], oxides, hydroxides, phosphides [15], chalcogenides [16], single-atom catalysts [17,18], and metal-organic frameworks [19,20], have been extensively exploited for OER electrocatalysis [21–23]. Among them, the nickel-iron-layered double hydroxides (NiFe-LDHs) have been demonstrated as one of the most promising candidates owing to their high OER performance and low costs [24–26]. However, their actual catalytic activity is still restricted by the inferior electrical conductivity and sluggish mass transfer. In previous reports, hydrothermal or solvothermal reactions are the most used methods in the fabrications of various NiFe-LDH materials [26–29]. Unfortunately, these methods are often time-consuming, requiring harsh

* Corresponding author.
** Corresponding author.
*** Corresponding author.
E-mail addresses: johnnyho@cityu.edu.hk (J.C. Ho), swdu@mju.edu.cn (S. Du), m.fang@szu.edu.cn (M. Fang).
[f] These authors contributed equally.

reaction conditions (such as high pressure and temperature), and sometimes releasing poisonous gases that are harmful to the environment and human health [30—34]. Moreover, for cost reduction, it is highly desirable that the catalysts are applicable and stable for working in electrolysis systems that are fed with highly accessible fresh water and/or seawater. However, investigations in such aspects are still insufficient [35,36].

In this article, we demonstrate the facile fabrication of a series of NiFe-LDH on carbon fiber cloth (CC) composites with different atomic ratios of Ni/Fe by applying a mild chemical method which was conducted under atmospheric pressure and a temperature below the boiling point of water. Despite the mild synthesizing condition, the obtained samples exhibit excellent electrocatalytic performance toward OER. It has been found that the NiFe-LDH/CC composites with a Ni/Fe atomic ratio of 6:4 possess the highest electrocatalytic activity, requiring an overpotential of only 226 mV and 238 mV in alkaline fresh water and seawater, respectively, which are much lower than those of the benchmarking RuO_2 catalyst for achieving a current density of 10 mA cm^{-1}. The same sample also exhibited robust stability and high selectivity for OER, showing no performance decay at a current density of 100 mA cm^{-2} for at least 160 h in 1 M KOH of seawater.

2. Experimental section

2.1. Preparation of NiFe-LDH-6-4/CC

The precursor solution was made by mixing 6 mmol of $NiCl_2 \cdot 6H_2O$, 4 mmol of $FeSO_4 \cdot 7H_2O$, 10 mmol of urea, and 50 ml of DI water in a glass bottle. Then, a piece of O_2 plasma-treated CC (0.8×3 cm^2) was submerged into the precursor solution with the upper half exposed to air. Next, the solution was heated to 90 °C and kept reacting for 4 h in an oil bath. After the reaction was finished, the system was cooled down to room temperature naturally. The sample was then taken out and rinsed with deionized (DI) water. Finally, the sample was dried at 60 °C in an electric oven overnight, and a dark brown CC sheet was acquired (Fig. S1a). Samples with different atomic ratios of Ni/Fe were obtained by adjusting the molar ratio of the Fe^{2+} and Ni^{2+} ions in the precursor solution. Detailed conditions of the O_2 plasma treatment of CC are given in the supporting information (SI).

2.2. Material characterization of NiFe-LDH/CC

X-ray diffraction (XRD) patterns of samples were collected on a Bruker-AXS D8 X-ray diffractometer with Cu-Kα radiation ($\lambda = 1.5406$ Å). The morphology of samples was observed by using scanning electron microscopes (SEMs) using TESCAN MIRA3, Zeiss Sigma 500, and Zeiss Merlin Compact microscopes, whereas the energy dispersive x-ray spectroscopy (EDS) mapping was collected on an Oxford X-MAX system. X-ray photoelectron spectroscopy (XPS) was performed on a Thermo Scientific Escalab 250Xi X-ray spectrometer. The transmission electron microscope (TEM) and selected area electron diffraction (SAED) were carried out using a Tecnai G2 F30/F20 JEOL-2100F TEM system at 200 kV. UV—vis absorption was performed on a PerkinElmer Lambda 1050+ UV/Vis/near-infrared spectrophotometer.

2.3. Electrochemical measurement

The electrochemical studies were conducted on a CHI 760E workstation (CHI, Shanghai, China) with a standard three-electrode system. A NiFe-LDH/CC sheet was used as the working electrode with a graphite rod as the counter electrode and a saturated calomel electrode (SCE, filled with saturated KCl solution) as the reference electrode. Cyclic voltammetry (CV) was used to determine OER activity, and the scan rate was 5 mV s^{-1}. The returned segments of the CV curves were used to analyze the overpotential at different current densities to exclude the influence from the oxidation peak of $Ni(OH)_2$ to NiOOH [37,38]. Chronopotentiometry was used to detect the OER stability under a constant current density of 100 mA cm^{-2}. The electrochemical impedance spectroscopy (EIS) was obtained at an overpotential of 340 mV in a frequency range from 0.01 Hz to 100 kHz with an amplitude of 5 mV. All the potentials versus SCE were converted to the reversible hydrogen electrode (RHE) with the Nernst equation ($E_{RHE} = E_{SCE} + 0.242 + 0.0591 \times pH$ (V)). The pH values of 1 M KOH solutions were determined to be 13.8 in water and 13.5 in seawater. All the electrochemical data as reported are internal resistance (iR)-compensated (90%) by deducting the potential caused by the solution resistance.
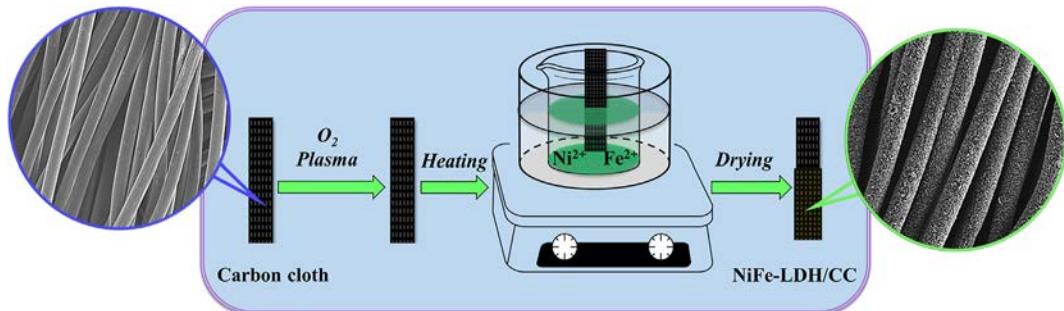
3. Results and discussion

3.1. Preparation and characterization of the NiFe-LDH/CC composites

To improve the hydrophilicity of substrates for effective loading of catalysts, CC is usually pretreated with strong oxidants, such as HNO_3, H_2SO_4, and $KMnO_4$, for several hours before use [39—41]. However, these strong oxidizing agents are toxic and environmentally harmful, whereas the involved processing methods are time-consuming. Here, we use an O_2 plasma processing scheme, which can modify the surface of CC to be hydrophilic in an efficient and eco-friendly manner. The preparation of NiFe-LDH/CC composites can be accomplished via two steps, including the pretreatment of CC with O_2 plasma for 60 s, followed by the direct growth of NiFe-LDH nanosheet arrays on CC in aqueous solutions containing urea and different molar ratios of Fe^{2+} and Ni^{2+} ions (Scheme 1). Through this method, the binder-free NiFe-LDH with hierarchical structures can be in situ grown on CC in 4 h, and no toxic gases are generated. The samples with Ni/Fe ratios of 0: 10, 2: 8, 4: 6, 6: 4, 8: 2, and 10: 0 were denoted as FeOH/CC, NiFe-LDH-2-8/CC, NiFe-LDH-4-6/CC, NiFe-LDH-6-4/CC, NiFe-LDH-8-2/CC, and NiOH/CC, respectively. Among them, NiFe-LDH-6-4/CC is selected as a representative for the description of characterization details.

The crystal structure of samples was characterized by XRD. For the pristine CC substrate, there are two main peaks located at $2\theta = 26.2$ and 44.2°, which correspond to the (002) and (101) diffraction of graphite (Fig. 1) [42,43]. The XRD patterns of NiOH/CC, NiFe-LDH-8-2/CC, NiFe-LDH-6-4/CC, and NiFe-LDH-4-6/CC exhibit a similar diffraction feature, where the diffraction peaks at $2\theta = 11.29, 22.82, 34.44, 38.99, 46.25, 59.84, 61.16$ and 65.26° can be indexed to the (003), (006), (012), (015), (018), (110), (113), and (116) planes of the standard NiFe-LDH phase (PDF#51-0463) [31,32,44]. Further increasing the Fe content causes a change of the crystal structure, and characteristic diffraction peaks of ferric oxide hydroxide (PDF#017-0536) are observed in the XRD patterns of the NiFe-LDH-2-8/CC and Fe—OH/CC samples.

The surface morphology and microstructure of pristine CC and NiFe-LDH-6-4/CC are first studied by the SEM. It can be observed that the CC is made of smooth carbon fibers with a diameter of about 10 μm (Fig. S1c). After the reaction, all the fibers are completely coated with a layer of three-dimensional (3D) NiFe-LDH arrays (Fig. 2a), indicating the intact contact of a NiFe-LDH layer on the CC substrate. The thickness of the layer is about 2—3 μm (Fig. S2a). In addition, there are abundant pores with the size ranging from the nanoscale to microscale formed in the layer (Fig. S2b), which offer rich channels and vast surface area for electrolyte exchanges and subsequent electrochemical reactions. The high-magnification SEM image (Fig. 2b) further reveals that the NiFe-LDH layer is composed of crossed-aligned nanosheet

Scheme 1. Schematic illustration of the synthetic procedure for NiFe-LDH/CC composites.
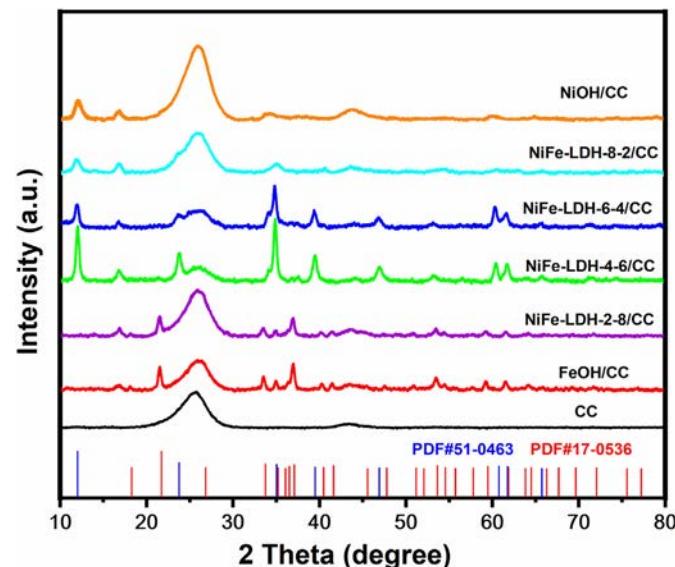

Fig. 1. XRD spectra of the NiFe-LDH/CC series with different Ni/Fe atomic ratios. (The standard XRD patterns of PDF#51-0463 and PDF#17-0536 are shown at the bottom).

arrays with sheet thickness ranging from 10 to 20 nm. At the same time, the EDS spectrum manifests the existence of C, O, Fe, and Ni elements in the resulting products (Fig. S3a) [45]. The elemental mappings were also collected, and the result confirmed the homogeneous distribution of Ni, Fe, and O across the carbon fibers without any noticeable segregation in the 3D layer (Fig. S3b), indicating the successful grafting of NiFe-LDH onto CC substrates. The Ni/Fe molar ratio of the NiFe-LDH layer was determined to be about 6: 4 which is well consistent with the starting Ni/Fe ratio of the precursor (Table S1). The effect of Ni/Fe molar ratios on the morphology of NiFe-LDH/CC samples was well-studied by the SEM (Fig. S4). For NiOH/CC, there was only a rough layer of material deposited onto the carbon fibers (Figs. S4a and b). At the molar ratio of Ni/Fe = 8: 2, plenty of small crossed-aligned nanosheets start to form (Figs. S4c and d). By increasing the Fe content to 4 mmol, the nanosheets became larger and more compactly packed (Figs. S4e and f). When the Ni/Fe molar ratio was set at 4: 6, many super-large NiFe-LDH nanosheets were observed in the form of random arrays (Figs. S4g and h, Fig. S5). Further increasing the proportion of Fe to 80% would then lead to the loose coating of overgrown Ni/Fe-LDH nanosheets on CC (Figs. S4i and j). In the case of FeOH/CC, vertically aligned nanorod arrays planted with bunches of mushroom-shaped particles are witnessed in the coating layer on the carbon fibers (Fig. S4k and l). These results indicate that NiFe-LDH-6-4/CC has the most uniform coating of ultrathin nanosheet arrays, which justify its highest electrocatalytic OER performance among all the samples in subsequent studies. The structure of nanosheets in the NiFe-LDH-6-4 layer was further confirmed by the TEM image (Fig. 2c).

The corresponding SAED pattern (inset in Fig. 2c) can be well indexed into the hexagonal LDH structure (PDF# 51-0463), which again confirms the high crystallinity of the sample. Meanwhile, in the high-resolution TEM image (Fig. 2d), lattice fringes with an interplanar distance of 0.143 nm were observed, which can be assigned to the (116) plane of the NiFe-LDH.

XPS was conducted to investigate the surface electronic states of the NiFe-LDH-6-4/CC composite (Fig. 3a). The peaks of Ni $2p_{3/2}$ and Ni $2p_{1/2}$ were detected at 856.3 eV and 873.9 eV (Fig. 3b), suggesting that the Ni was predominantly in a divalent state [44]. The XPS spectrum of Fe $2p$ (Fig. 3c) exhibits the two prominent peaks at 712.6 eV and 726.2 eV for the Fe $2p_{3/2}$ and Fe $2p_{1/2}$ components with a peak separation of ~14 eV, affirming the presence of Fe^{3+} in NiFe-LDH-6-4/CC [46]. In the spectrum of O $1s$, there are two peaks positioned at 531.2 eV and 532.2 eV (Fig. 3d). The former corresponds to the binding energy of metal O, whereas the latter can be assigned to the metal OH in NiFe-LDH [47].

3.2. OER properties of the NiFe-LDH/CC composites

The electrocatalytic OER performance of NiFe-LDH/CC composites is determined in a classical three-electrode set up in a 1 M KOH solution. The samples were partially covered with an insulating and corrosion-resistant silicone rubber sealant to define an exposed area of about 0.8 cm^2 (Fig. S1b). Before measurement, CV scans are performed until the steady CV characteristics are observed. As previously reported, the Ni/Fe atomic ratio of the precursor solution has a great impact on the OER activity of NiFe-based electrocatalysts [48–50]. Here, we systematically investigate the OER activity of NiFe-LDH/CC samples prepared from the precursor solutions of various Ni/Fe ratios. As shown in Fig. 4a, there are remarkable changes in the OER activity of NiFe-LDH/CC when increasing the Ni/Fe ratios. For a better comparison, their OER overpotential values at the current densities of 10, 50, and 100 mA cm^{-2} are depicted in Fig. 4b, which presents an obvious trend of first decreasing and then increasing on the OER overpotential on increasing the Ni/Fe ratio. Among all the samples, the lowest overpotential is attained for the NiFe-LDH-6-4/CC sample at all three current densities. In alkaline aqueous solution, NiFe-LDH-6-4/CC can deliver current densities of 10 and 100 mA cm^{-2} at overpotentials of merely 226 and 252 mV, respectively. These values are lower than those of the recently reported NiFe-LDH-based electrocatalysts and the commercial RuO$_2$ powder that is often used as the benchmarking catalyst for OER (Fig. 4a and Table S2). Tafel plots derived from the OER polarization curve are important intrinsic identities of electrocatalysts. The lower Tafel slope infers to the higher achievable current density at a given overpotential. To better evaluate the OER reaction kinetics, corresponding Tafel slopes derived from linear sweep voltammetry (LSV) curves of the NiFe-LDH/CC samples are shown in Fig. S6, and the Tafel slope values are plotted in Fig. 4c. In specific, the NiFe-
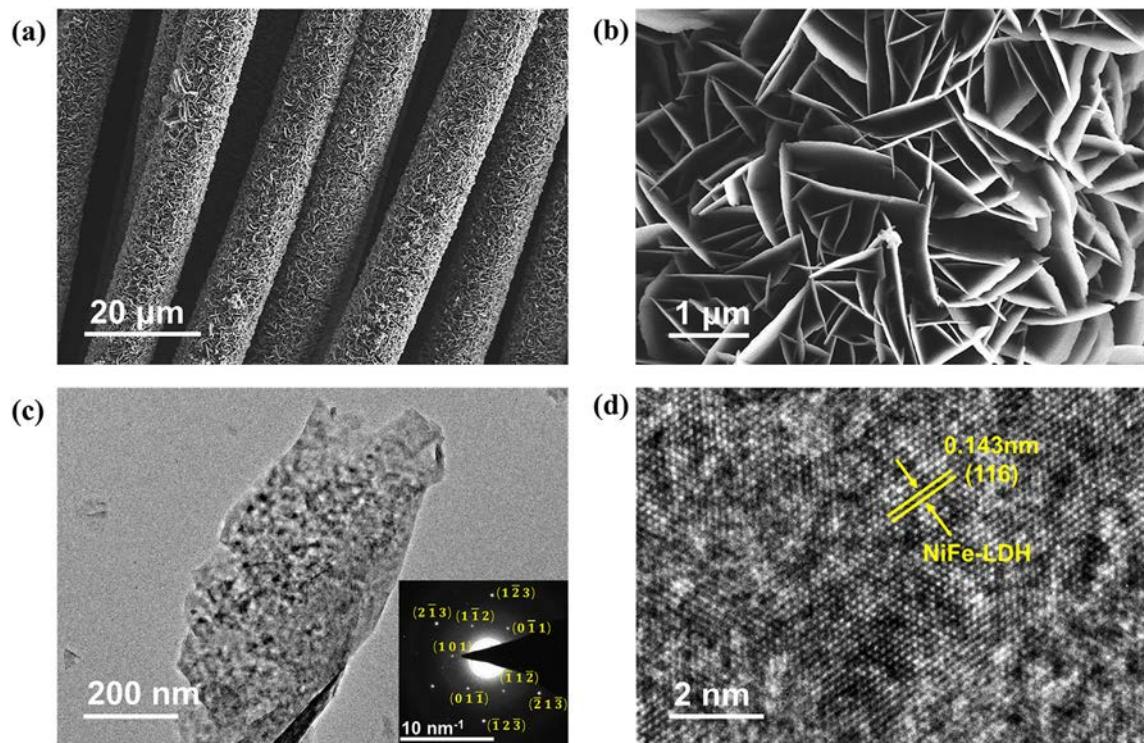
Fig. 2. (**a**) SEM, (**b**) high-magnification SEM, (**c**) TEM, and (**d**) HRTEM images of the prepared NiFe-LDH-6-4/CC. The inset in (**c**) shows the SAED pattern.
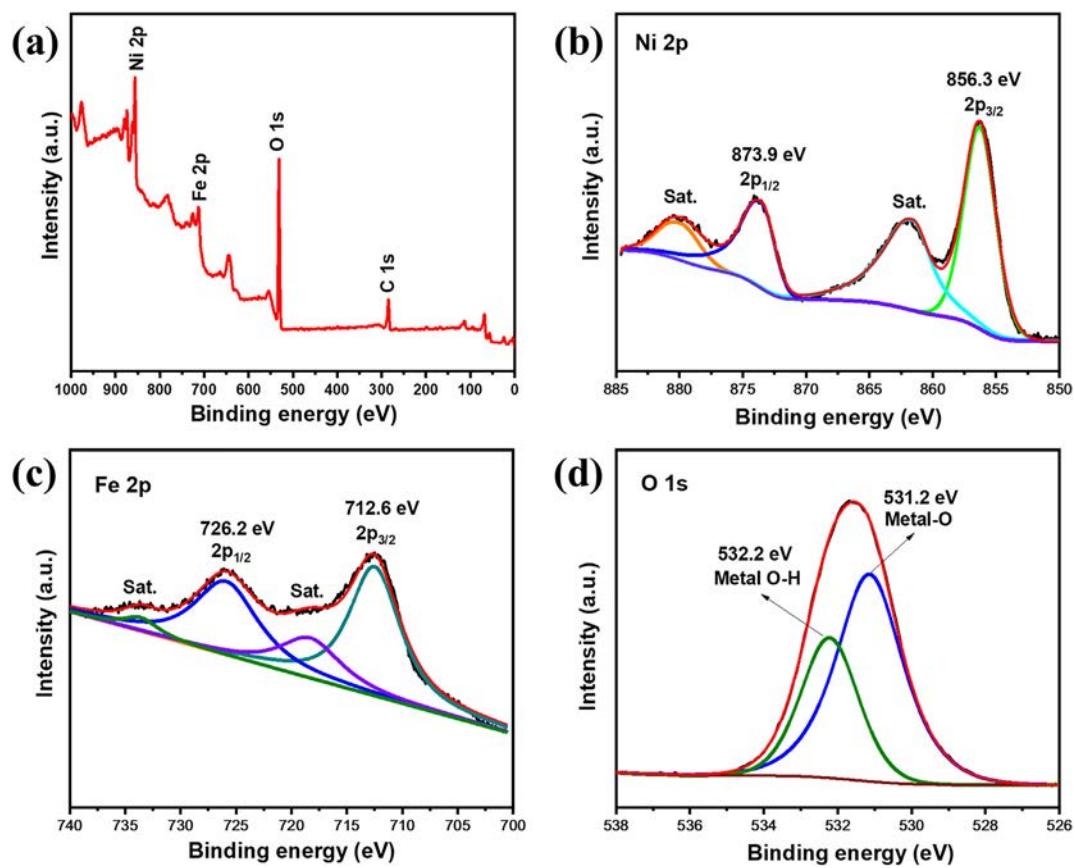

Fig. 3. XPS spectrum survey (**a**), and the high-resolution XPS spectra of Ni 2p (**b**), Fe 2p (**c**), O 1s (**d**) of NiFe-LDH-6-4/CC.
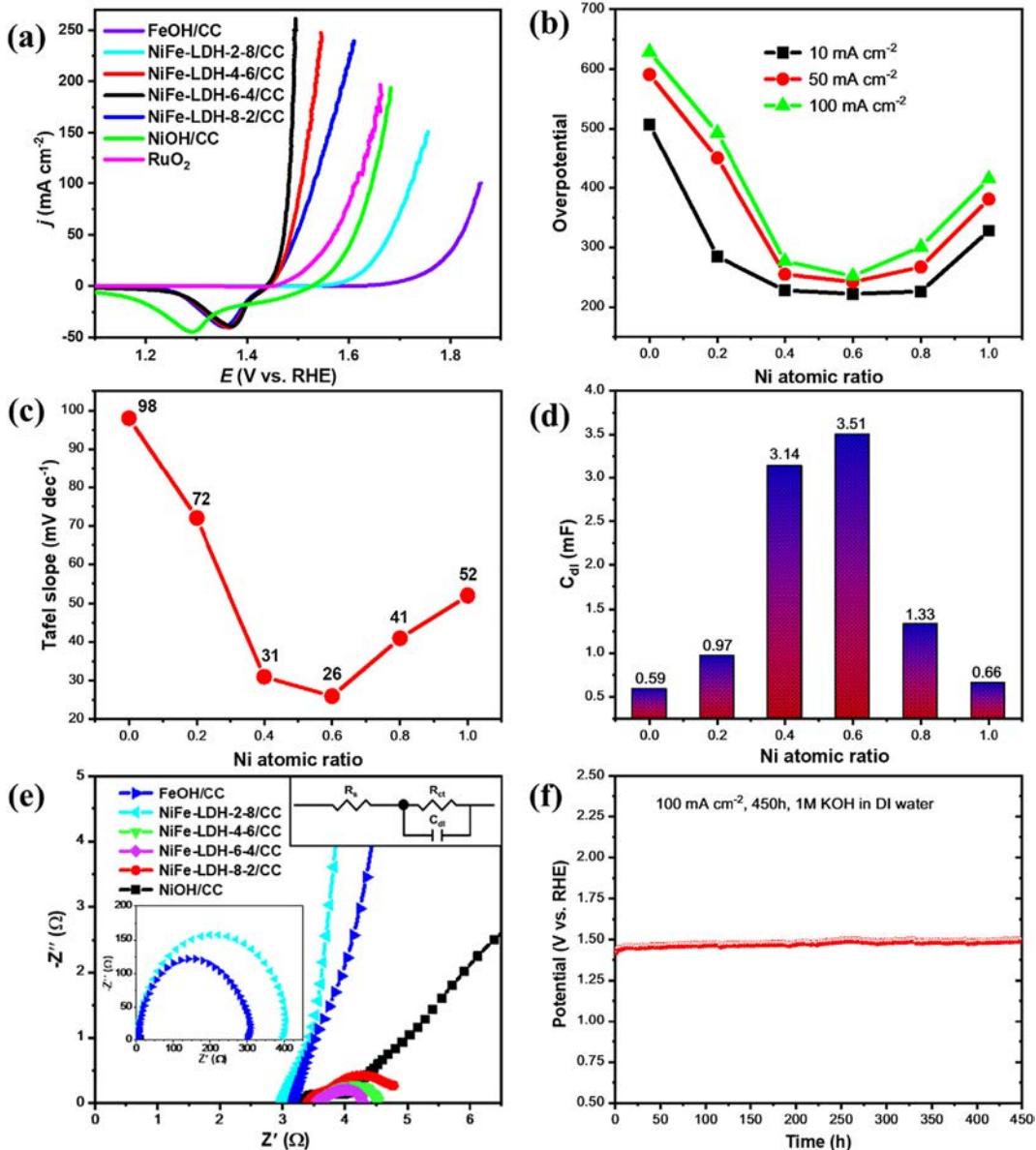
Fig. 4. (**a**) The OER polarization curves of NiFe-LDH/CC composites and RuO$_2$ at a scan rate of 5 mV s^{-1}, (**b**) the variation trends of overpotential at current densities of 10, 50, or 100 mA cm^{-2}, (**c**) corresponding Tafel slope changes derived from OER polarization curves, (**d**) the C$_{dl}$ values, (**e**) the Nyquist plots and the equivalent circuit at an overpotential of 340 mV for the NiFe-LDH/CC composites, and (**f**) the chronopotentiometry measurement at a current density of 100 mA cm^{-2} for the NiFe-LDH-6-4/CC. All data are collected in the 1 M KOH electrolyte in DI water.

LDH-6-4/CC sample exhibits the smallest Tafel slope of 26 mV dec^{-1} among all the samples, indicating more favorable OER kinetics for the NiFe-LDH-6-4/CC electrode. The enhanced OER activity of NiFe-LDH-6-4/CC can be attributed to its more optimized electronic structure associated with the partial electronic redistribution among Ni and Fe atoms by bridging O^{2-} and its larger active site area, which facilitates the charge transfer and improves the adsorption/desorption capacity of oxygenated species on the catalyst surface [51,52].

To further investigate the intrinsic electrocatalytic activity of the NiFe-LDH/CC, the electrochemical active surface area (ECSA) was determined from the double-layer capacitance (C$_{dl}$) derived from the non-Faradaic region in the CV measurement [53]. Explicitly, CV curves at different scan rates are recorded (potential range: −0.05 ~ +0.05 V versus SCE) to obtain the capacitive current related to C$_{dl}$ for the NiFe-LDH/CC samples (Fig. S7). Then, the C$_{dl}$ value can be obtained by plotting $\Delta j/2 = (j_a - j_c)/2$ at 0 V (vs SCE)

against the scan rate, where j_a and j_c are the anodic and cathodic currents, respectively. The variation trend of C$_{dl}$ to the concentration of Ni is depicted in Fig. 4d. The largest C$_{dl}$ value of 3.51 mF is acquired for NiFe-LDH-6-4/CC, which should be responsible for its superior electrocatalytic OER activity. In other words, the NiFe-LDH-6-4/CC composite has the largest ECSA among all samples with varied Ni/Fe ratios, where this enhanced surface area can be attributed to their cross-aligned ultrathin nanosheet arrays, providing richer channels and more active sites for favorable electrode reactions. Although the ECSA is a critical factor, it is not the only one determining the activity of catalysts. In this way, it is also essential to explore the charge transfer kinetics involved in the OER process by recording the electrochemical impedance spectra (EIS) of NiFe-LDH/CC composites at 1.57 V versus RHE [46,54,55]. The related Nyquist plots and equivalent circuits are shown in Fig. 4e. All the samples display similar Nyquist plots with apparent semicircles, corresponding to the charge transfer resistance (R$_{ct}$).
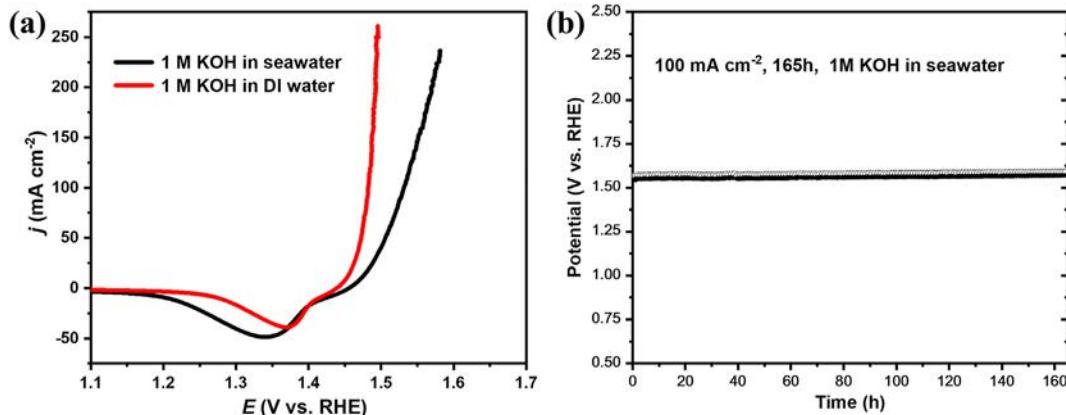
Fig. 5. (**a**) OER polarization plots of NiFe-LDH-6-4/CC at a scan rate of 5 mV s^{-1} in the 1 M KOH electrolyte (seawater and DI water) and (**b**) chronopotentiometry measurement for NiFe-LDH-6-4/CC at a current density of 100 mA cm^{-2}.

The semicircles of FeOH/CC and NiOH/CC are much bigger than those of other samples, implying their much higher charge transfer resistance in the OER process. The EIS data are then fitted to the equivalent circuit, and the fitting parameters are listed in Table S3, which reveals the slight difference in resistance (R_s) but great disparity among the R_{ct} values for the samples. It can be observed that, except NiFe-LDH/CC-2-8, FeOH/CC, and NiOH/CC, the other NiFe-LDH/CC samples show low R_{ct} values, suggesting their much faster charge transfer rate during the OER process [38]. The smallest R_{ct} of 0.24 Ω is observed on NiFe-LDH-6-4/CC, implying its lowest electronic resistance at the electrode/electrolyte interface. The EIS results are in good consistency with the Tafel slopes of the samples, confirming that the charge transfer kinetics also play a crucial role in the process of OER.
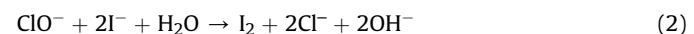
Besides the catalytic activity, high stability is also an essential requirement for OER catalysts. In this work, the evaluation of the OER stability of NiFe-LDH-6-4/CC is conducted by chronopotentiometry at a current density of 100 mV cm^{-2}, and the result is compiled in Fig. 4f. After 450 h of OER in 1 M KOH solution, the applied potential increases only 65 mV. Obviously, NiFe-LDH-6-4/CC shows high OER stability and surpasses the stability on most of the OER catalysts reported recently [51,56]. The morphology of NiFe-LDH-6-4/CC after 450 h chronopotentiometry test reveals that the overall cross-aligned nanosheet arrays are still well preserved (Fig. S8), just with some cracks on the surface, which may be resulted from the long-time impact of releasing O_2 at a fast rate. Meanwhile, parts of the nanosheet arrays are covered by some flakes or particles, which may block the mass transfer during the OER process and decrease the OER stability accordingly. Nevertheless, the crystal phase of the catalyst was well preserved, as confirmed by both the TEM image and XRD pattern recorded after the chronopotentiometry test (Fig. S9). Faraday efficiency (FE) is an important index to evaluate the actual productivity for HER or OER in water splitting [57]. Here, the FE of OER on NiFe-LDH-6-4/CC is measured by a drainage method and determined to be 97.7%, implying a very high OER productivity (more details can be seen in the SI). Such a high OER performance of NiFe-LDH-6-4/CC can be attributed to the robust structure of NiFe-LDH-6-4 nanosheets and the strong bonding between the NiFe-LDH layer and CC substrate.

3.3. OER activity of NiFe-LDH-6-4/CC in seawater

For practical considerations, seawater electrolysis is an ideal future technology that can be used for both hydrogen generation and seawater desalination [58,59]. It is of great importance for energy storage and freshwater harvesting from the ocean. In this case,

the performance of NiFe-LDH-6-4/CC on seawater electrolysis is investigated, and the results are presented in Fig. 5. To deliver a current density of 100 mA cm^{-2}, the overpotential required is just 301 mV (Fig. 5a), and the OER potential increment is only 33 mV after 165 h of seawater electrolysis at the current density of 100 mA cm^{-2} (Fig. 5b). The OER performance of the NiFe-LDH-6-4/CC composite in seawater is not so good as that in the freshwater, but it still shows good activity and distinguished stability in seawater splitting. These performances are also among the best of recently reported OER electrocatalysts for seawater splitting under real or simulated seawater electrolyte conditions (Table S4 and Fig. S10). In addition, the FE for OER in seawater is calculated to be as high as 96.9%, which is only slightly lower than that in DI water. The previous results are very meaningful for the scalable application of the NiFe-LDH catalysts in hydrogen harvesting from seawater.

It was known that in the electrolysis of chloride-containing electrolytes, chlorine evolution reaction (CER) may coexist with OER [60,61], which will lower the OER efficiency and cause harm to the environment and people's health [62]. Thus, the influence of CER should be put into consideration in the OER process of seawater. Here, a titration method coupled with absorption spectrometry was used to determine whether Cl_2 is produced in OER [63]. Potassium iodide (KI) is used as the reductant and will be oxidized into I_2 by ClO^- generated from the reaction of Cl_2 and OH^- in the electrolyzed solution (Eq. (1) & (2)). The I_2 formed will then show an absorption peak at 440 nm [63]. The electrolyzed seawater after the stability test was used to examine the evolution of Cl_2, and more details are provided in the SI. As shown in Fig. S11, the absorption spectra of the electrolysis solution show no absorption peak attributed to I_2, indicating that no Cl_2 is generated during the seawater electrolysis, proving that the CER was fully suppressed under the electrolysis condition. Combined with its OER performance in activity and stability, NiFe-LDH-6-4/CC is of great potential in seawater splitting for harvesting hydrogen energy.

$$Cl_2 + 2OH^- \rightarrow ClO^- + Cl^- + H_2O \tag{1}$$

$$ClO^- + 2I^- + H_2O \rightarrow I_2 + 2Cl^- + 2OH^- \tag{2}$$

4. Conclusion

In conclusion, we have reported a facile method to prepare a series of NiFe-LDH nanosheets with various Ni/Fe molar ratios on the carbon cloth under mild conditions (90 °C, atmospheric pressure), and the OER activity and stability in both fresh water and seawater are well investigated. The stoichiometric ratio of Ni and Fe

has a strong impact on shaping the nanostructure of the catalysts and hence the OER performance. The optimized Ni/Fe ratio of the catalysts was found to be 6: 4, which led to NiFe-LDH-6-4/CC with more dense and uniform arrays of NiFe-LDH nanosheets on the carbon fibers. Consequently, it shows the better OER performance with lower overpotentials, smaller Tafel slope and R_{ct}, and larger C_{dl} values compared with those having other Ni/Fe ratios. It also exhibits a satisfactory OER durability up to 450 h in fresh water and 165 h in seawater at the current density of 100 mA cm^{-2}. The facile fabrication and high performance of these hybrid materials present great promise of earth-abundant OER catalysts in meeting the criteria of activity, durability, selectivity, and cost for practical seawater electrolysis.

Author contributions

Guofa Dong: conceptualization, methodology, investigation, writing — original draft. **Fengyan Xie:** methodology, investigation. **Fangxia Kou:** methodology, investigation. **Tingting Chen:** data curation, validation. **Fengyun Wang:** data curation, validation. **Yingwu Zhou:** software. **Kechen Wu:** data curation, project administration. **Shaowu Du:** conceptualization, supervision, funding acquisition. **Ming Fang:** conceptualization, methodology, writing — reviewing and editing. **Johnny C. Ho:** conceptualization, writing — reviewing and editing, supervision, funding acquisition.

Declaration of competing interest

The authors declare that they have no known competing financial interests or personal relationships that could have appeared to influence the work reported in this article.

Acknowledgments

Appendix A. Supplementary data

Supplementary data to this article can be found online at https://doi:10.1016/j.mtener.2021.100883.

References

[1] J.O. Abe, A.P.I. Popoola, E. Ajenifuja, O.M. Popoola, Hydrogen energy, economy and storage: review and recommendation, Int. J. Hydrogen Energy 44 (2019) 15072–15086, https://doi.org/10.1016/j.ijhydene.2019.04.068.

[2] A. Kovač, M. Paranos, D. Marciuš, Hydrogen in energy transition: a review, Int. J. Hydrogen Energy 46 (2021) 10016–10035, https://doi.org/10.1016/j.ijhydene.2020.11.256.

[3] M.A. Rosen, S. Koohi-Fayegh, The prospects for hydrogen as an energy carrier: an overview of hydrogen energy and hydrogen energy systems, Energy Ecol. Environ. 1 (2016) 10–29, https://doi.org/10.1007/s40974-016-0005-z.

[4] K.T. Møller, T.R. Jensen, E. Akiba, H.-w. Li, Hydrogen - a sustainable energy carrier, Prog. Nat. Sci. 27 (2017) 34–40, https://doi.org/10.1016/j.pnsc.2016.12.014.

[5] I. Staffell, D. Scamman, A. Velazquez Abad, P. Balcombe, P.E. Dodds, P. Ekins, N. Shah, K.R. Ward, The role of hydrogen and fuel cells in the global energy system, Energy Environ. Sci. 12 (2019) 463–491, https://doi.org/10.1039/C8EE01157E.

[6] M. Carmo, D.L. Fritz, J. Mergel, D. Stolten, A comprehensive review on PEM water electrolysis, Int. J. Hydrogen Energy 38 (2013) 4901–4934, https://doi.org/10.1016/j.ijhydene.2013.01.151.

[7] J. Chi, H. Yu, Water electrolysis based on renewable energy for hydrogen production, Chin. J. Catal. 39 (2018) 390–394, https://doi.org/10.1016/S1872-2067(17)62949-8.

[8] P. Nikolaidis, A. Poullikkas, A comparative overview of hydrogen production processes, Renew. Sustain. Energy Rev. 67 (2017) 597–611, https://doi.org/10.1016/j.rser.2016.09.044.

[9] Z. Zhou, Z. Pei, L. Wei, S. Zhao, X. Jian, Y. Chen, Electrocatalytic hydrogen evolution under neutral pH conditions: current understandings, recent advances, and future prospects, Energy Environ. Sci. 13 (2020) 3185–3206, https://doi.org/10.1039/D0EE01856B.

[10] A. Buttler, H. Spliethoff, Current status of water electrolysis for energy storage, grid balancing and sector coupling *via* power-to-gas and power-to-liquids: a review, Renew. Sustain. Energy Rev. 82 (2018) 2440–2454, https://doi.org/10.1016/j.rser.2017.09.003.

[11] M. Wang, Z. Wang, X. Gong, Z. Guo, The intensification technologies to water electrolysis for hydrogen production − a review, Renew. Sustain. Energy Rev. 29 (2014) 573–588, https://doi.org/10.1016/j.rser.2013.08.090.

[12] J. Kibsgaard, I. Chorkendorff, Considerations for the scaling-up of water splitting catalysts, Nat. Energy 4 (2019) 430–433, https://doi.org/10.1038/s41560-019-0407-1.

[13] M.I. Jamesh, Y. Kuang, X. Sun, Constructing earth-abundant 3D nanoarrays for efficient overall water splitting—A review, ChemCatChem 11 (2019) 1550–1575, https://doi.org/10.1002/cctc.201801783.

[14] H. Lei, Z. Wang, F. Yang, X. Huang, J. Liu, Y. Liang, J. Xie, M.S. Javed, X. Lu, S. Tan, W. Mai, NiFe nanoparticles embedded N-doped carbon nanotubes as high-efficient electrocatalysts for wearable solid-state Zn-air batteries, Nanomater. Energy 68 (2020) 104293, https://doi.org/10.1016/j.nanoen.2019.104293.

[15] C. Teng, N. Zhang, X. Gao, X. Li, Z. Wu, W. Wang, M. Zhi, Z. Hong, Uniform NiFe phosphide nanosheets arrays on carbon cloth as high-performance oxygen evolution catalysts, Mater, Today Energy 11 (2019) 192–198, https://doi.org/10.1016/j.mtener.2018.11.008.

[16] X. Zhang, Y. Xue, Q. Yan, K. Zhu, K. Ye, J. Yan, D. Cao, X. Huang, G. Wang, Hydrangea-like sulfide NiFe layered double hydroxides grown on an undulate nickel framework as bifunctional electrocatalysts for overall water splitting, Mater, Today Energy 21 (2021) 100741, https://doi.org/10.1016/j.mtener.2021.100741.

[17] Y. Yang, Z. Pei, K.-H. Wu, C. Tan, H. Wang, L. Wei, A. Mahmood, C. Yan, J. Dong, S. Zhao, Y. Chen, Recent progress of carbon-supported single-atom catalysts for energy conversion and storage, Matter 3 (2020) 1442–1476, https://doi.org/10.1016/j.matt.2020.07.032.

[18] Y. Wang, F.-L. Hu, Y. Mi, C. Yan, S. Zhao, Single-metal-atom catalysts: an emerging platform for electrocatalytic oxygen reduction, Chem. Eng. J. 406 (2021) 127135, https://doi.org/10.1016/j.cej.2020.127135.

[19] S. Zhao, C. Tan, C.-T. He, P. An, F. Xie, S. Jiang, Y. Zhu, K.-H. Wu, B. Zhang, H. Li, J. Zhang, Y. Chen, S. Liu, J. Dong, Z. Tang, Structural transformation of highly active metal−organic framework electrocatalysts during the oxygen evolution reaction, Nat. Energy 5 (2020) 881–890, https://doi.org/10.1038/s41560-020-00709-1.

[20] H. Lei, Y. Liang, G. Cen, B.-t. Liu, S. Tan, Z. Wang, W. Mai, Atomic layer deposited Al₂O₃ layer confinement: an efficient strategy to synthesize durable MOF-derived catalysts toward the oxygen evolution reaction, Inorg. Chem. Front. 8 (2021) 1432–1438, https://doi.org/10.1039/D0QI01317J.

[21] L. Han, S. Dong, E. Wang, Transition-metal (Co, Ni, and Fe)-Based electrocatalysts for the water oxidation reaction, Adv. Mater. 28 (2016) 9266–9291, https://doi.org/10.1002/adma.201602270.

[22] M.-I. Jamesh, X. Sun, Recent progress on earth abundant electrocatalysts for oxygen evolution reaction (OER) in alkaline medium to achieve efficient water splitting—A review, J. Power Sources 400 (2018) 31–68, https://doi.org/10.1016/j.jpowsour.2018.07.125.

[23] J. Zhao, J.J. Zhang, Z.Y. Li, X.H. Bu, Recent progress on NiFe-based electrocatalysts for the oxygen evolution reaction, Small 16 (2020) 2003916, https://doi.org/10.1002/smll.202003916.

[24] X. Lu, H. Xue, H. Gong, M. Bai, D. Tang, R. Ma, T.J.N.-M.L. Sasaki, 2D layered double hydroxide nanosheets and their derivatives toward efficient oxygen evolution reaction, Nano-Micro Lett. 12 (2020) 1–32, https://doi.org/10.1007/s40820-020-00421-5.

[25] Y. Wang, D. Yan, S. El Hankari, Y. Zou, S. Wang, Recent progress on layered double hydroxides and their derivatives for electrocatalytic water splitting, Adv. Sci. 5 (2018) 1800064, https://doi.org/10.1002/advs.201800064.

[26] S. Anantharaj, K. Karthick, S. Kundu, Evolution of layered double hydroxides (LDH) as high performance water oxidation electrocatalysts: a review with insights on structure, activity and mechanism, Mater. Today Energy 6 (2017) 1–26, https://doi.org/10.1016/j.mtener.2017.07.016.

[27] P.M. Bodhankar, P.B. Sarawade, G. Singh, A. Vinu, D.S. Dhawale, Recent advances in highly active nanostructured NiFe LDH catalyst for electrochemical water splitting, J. Mater. Chem. 9 (2021) 3180–3208, https://doi.org/10.1039/D0TA10712C.

[28] Z. Cai, X. Bu, P. Wang, J.C. Ho, J. Yang, X. Wang, Recent advances in layered double hydroxide electrocatalysts for the oxygen evolution reaction, J. Mater. Chem. 7 (2019) 5069–5089, https://doi.org/10.1039/C8TA11273H.

[29] L. Wu, L. Yu, X. Xiao, F. Zhang, S. Song, S. Chen, Z. Ren, Recent advances in self-supported layered double hydroxides for oxygen evolution reaction, Research 2020 (2020) 3976278, https://doi.org/10.34133/2020/3976278.

[30] F. Dionigi, T. Reier, Z. Pawolek, M. Gliech, P. Strasser, Design criteria, operating conditions, and nickel-iron hydroxide catalyst materials for selective seawater electrolysis, ChemSusChem 9 (2016) 962−972, https://doi.org/10.1002/cssc.201501581.

[31] M. Gong, Y. Li, H. Wang, Y. Liang, J.Z. Wu, J. Zhou, J. Wang, T. Regier, F. Wei, H. Dai, An advanced Ni−Fe layered double hydroxide electrocatalyst for water oxidation, J. Am. Chem. Soc. 135 (2013) 8452−8455, https://doi.org/10.1021/ja4027715.

[32] Y. Ma, Y. Wang, D. Xie, Y. Gu, H. Zhang, G. Wang, Y. Zhang, H. Zhao, P.K. Wong, NiFe-layered double hydroxide nanosheet arrays supported on carbon cloth for highly sensitive detection of nitrite, ACS Appl. Mater. Interfaces 10 (2018) 6541−6551, https://doi.org/10.1021/acsami.7b16536.

[33] F.-S. Zhang, J.-W. Wang, J. Luo, R.-R. Liu, Z.-M. Zhang, C.-T. He, T.-B. Lu, Extraction of nickel from NiFe-LDH into Ni₂P@NiFe hydroxide as a bifunctional electrocatalyst for efficient overall water splitting, Chem. Sci. 9 (2018) 1375−1384, https://doi.org/10.1039/C7SC04569G.

[34] H. Zhang, X. Li, A. Hähnel, V. Naumann, C. Lin, S. Azimi, S.L. Schweizer, A.W. Maijenburg, R.B. Wehrspohn, Bifunctional heterostructure assembly of NiFe LDH nanosheets on NiCoP nanowires for highly efficient and stable overall water splitting, Adv. Funct. Mater. 28 (2018) 1706847, https://doi.org/10.1002/adfm.201706847.

[35] S.R. Dresp, F. Dionigi, M. Klingenhof, P. Strasser, Direct electrolytic splitting of seawater: opportunities and challenges, ACS Energy Lett. 4 (2019) 933−942, https://doi.org/10.1021/acsenergylett.9b00220.

[36] F. Zhang, L. Yu, L. Wu, D. Luo, Z. Ren, Rational design of oxygen evolution reaction catalysts for seawater electrolysis, Trends Environ. Anal. Chem. 3 (2021) 485−498, https://doi.org/10.1016/j.trechm.2021.03.003.

[37] G. Dong, M. Fang, J. Zhang, R. Wei, L. Shu, X. Liang, S. Yip, F. Wang, L. Guan, Z. Zheng, J.C. Ho, *In situ* formation of highly active Ni−Fe based oxygen-evolving electrocatalysts *via* simple reactive dip-coating, J. Mater. Chem. 5 (2017) 11009−11015, https://doi.org/10.1039/C7TA01134B.

[38] C.C.L. McCrory, S. Jung, I.M. Ferrer, S.M. Chatman, J.C. Peters, T.F. Jaramillo, Benchmarking hydrogen evolving reaction and oxygen evolving reaction electrocatalysts for solar water splitting devices, J. Am. Chem. Soc. 137 (2015) 4347−4357, https://doi.org/10.1021/ja510442p.

[39] H. Hu, S. Wageh, A.A. Al-Ghamdi, S. Yang, Z. Tian, B. Cheng, W. Ho, NiFe-LDH nanosheet/carbon fiber nanocomposite with enhanced anionic dye adsorption performance, Appl. Surf. Sci. 511 (2020) 145570, https://doi.org/10.1016/j.apsusc.2020.145570.

[40] M. Li, H. Li, X. Jiang, M. Jiang, X. Zhan, G. Fu, J.-M. Lee, Y. Tang, Gd-induced electronic structure engineering of a NiFe-layered double hydroxide for efficient oxygen evolution, J. Mater. Chem. 9 (2021) 2999−3006, https://doi.org/10.1039/D0TA10740A.

[41] R. Li, J. Xu, Q. Pan, J. Ba, T. Tang, W. Luo, One-Step synthesis of NiFe layered double hydroxide nanosheet array/N-doped graphite foam electrodes for oxygen evolution reactions, ChemistryOpen 8 (2019) 1027−1032, https://doi.org/10.1002/open.201900190.

[42] Y. Wei, R. Wang, L. Meng, Y. Wang, G. Li, S. Xin, X. Zhao, K. Zhang, Hydrogen generation from alkaline NaBH₄ solution using a dandelion-like Co−Mo−B catalyst supported on carbon cloth, Int. J. Hydrogen Energy 42 (2017) 9945−9951, https://doi.org/10.1016/j.ijhydene.2016.12.130.

[43] S. Meng, Y. Hong, Z. Dai, W. Huang, X. Dong, Simultaneous detection of dihydroxybenzene isomers with ZnO nanorod/carbon cloth electrodes, ACS Appl. Mater. Interfaces 9 (2017) 12453−12460, https://doi.org/10.1021/acsami.7b00546.

[44] F. Wang, T. Wang, S. Sun, Y. Xu, R. Yu, H. Li, One-step synthesis of Nickle Iron-layered double hydroxide/reduced graphene oxide/carbon nanofibres composite as electrode materials for asymmetric supercapacitor, Sci. Rep. 8 (2018) 8908, https://doi.org/10.1038/s41598-018-27171-0.

[45] B.M. Hunter, W. Hieringer, J.R. Winkler, H.B. Gray, A.M. Müller, Effect of interlayer anions on [NiFe]-LDH nanosheet water oxidation activity, Energy Environ. Sci. 9 (2016) 1734−1743, https://doi.org/10.1039/C6EE00377J.

[46] Y. Lin, H. Wang, C.-K. Peng, L. Bu, C.-L. Chiang, K. Tian, Y. Zhao, J. Zhao, Y.-G. Lin, J.-M. Lee, L. Gao, Co-induced electronic optimization of hierarchical NiFe LDH for oxygen evolution, Small 16 (2020) 2002426, https://doi.org/10.1002/smll.202002426.

[47] A.A. Kashale, C.-H. Yi, K.-Y. Cheng, J.-S. Guo, Y.-H. Pan, I.W.P. Chen, Binder-free heterostructured NiFe₂O₄/NiFe LDH nanosheet composite electrocatalysts for oxygen evolution reactions, ACS Appl. Energy Mater. 3 (2020) 10831−10840, https://doi.org/10.1021/acsaem.0c01863.

[48] X.F. Lu, L. Yu, X.W.D. Lou, Highly crystalline Ni-doped FeP/carbon hollow nanorods as all-pH efficient and durable hydrogen evolving electrocatalysts, Sci. Adv. 5 (2019) eaav6009, https://doi.org/10.1126/sciadv.aav6009.

[49] A.M.P. Sakita, E. Vallés, R.D. Noce, A.V. Benedetti, Novel NiFe/NiFe-LDH composites as competitive catalysts for clean energy purposes, Appl. Surf. Sci. 447 (2018) 107−116, https://doi.org/10.1016/j.apsusc.2018.03.235.

[50] D. Zhou, Y. Jia, X. Duan, J. Tang, J. Xu, D. Liu, X. Xiong, J. Zhang, J. Luo, L. Zheng, B. Liu, Y. Kuang, X. Sun, X. Duan, Breaking the symmetry: gradient in NiFe layered double hydroxide nanoarrays for efficient oxygen evolution, Nanomater. Energy 60 (2019) 661−666, https://doi.org/10.1016/j.nanoen.2019.04.014.

[51] H. Li, Q. Zhou, F. Liu, W. Zhang, Z. Tan, H. Zhou, Z. Huang, S. Jiao, Y. Kuang, Biomimetic design of ultrathin edge-riched FeOOH@Carbon nanotubes as high-efficiency electrocatalysts for water splitting, Appl. Catal. B Environ. 255 (2019) 117755, https://doi.org/10.1016/j.apcatb.2019.117755.

[52] Y. Liu, S. Liu, Y. Wang, Q. Zhang, L. Gu, S. Zhao, D. Xu, Y. Li, J. Bao, Z. Dai, Ru modulation effects in the synthesis of unique rod-like Ni@Ni₂P−Ru heterostructures and their remarkable electrocatalytic hydrogen evolution performance, J. Am. Chem. Soc. 140 (2018) 2731−2734, https://doi.org/10.1021/jacs.7b12615.

[53] J. Zhang, L. Yu, Y. Chen, X.F. Lu, S. Gao, X.W. Lou, Designed formation of double-shelled Ni−Fe layered-double-hydroxide nanocages for efficient oxygen evolution reaction, Adv. Mater. 32 (2020) 1906432, https://doi.org/10.1002/adma.201906432.

[54] Y. Zou, B. Xiao, J.-W. Shi, H. Hao, D. Ma, Y. Lv, G. Sun, J. Li, Y. Cheng, 3D hierarchical heterostructure assembled by NiFe LDH/(NiFe)Sₓ on biomass-derived hollow carbon microtubes as bifunctional electrocatalysts for overall water splitting, Electrochim. Acta 348 (2020) 136339, https://doi.org/10.1016/j.electacta.2020.136339.

[55] C.Y. Chang, A.A. Kashale, C.M. Lee, S.L. Chu, Y.F. Lin, I.W.P. Chen, Single atomically anchored iron on graphene quantum dots for a highly efficient oxygen evolution reaction, Mater, Today Energy 20 (2021) 100693, https://doi.org/10.1016/j.mtener.2021.100693.

[56] N.-T. Suen, S.-F. Hung, Q. Quan, N. Zhang, Y.-J. Xu, H.M. Chen, Electrocatalysis for the oxygen evolution reaction: recent development and future perspectives, Chem. Soc. Rev. 46 (2017) 337−365, https://doi.org/10.1039/C6CS00328A.

[57] M. Görlin, P. Chernev, J. Ferreira de Araújo, T. Reier, S. Dresp, B. Paul, R. Krähnert, H. Dau, P. Strasser, Oxygen evolution reaction dynamics, faradaic charge efficiency, and the active metal redox states of Ni−Fe oxide water splitting electrocatalysts, J. Am. Chem. Soc. 138 (2016) 5603−5614, https://doi.org/10.1021/jacs.6b00332.

[58] L. Yu, L. Wu, S. Song, B. McElhenny, F. Zhang, S. Chen, Z. Ren, Hydrogen generation from seawater electrolysis over a sandwich-like NiCoN| NiₓP| NiCoN microsheet array catalyst, ACS Energy Lett. 5 (2020) 2681−2689, https://doi.org/10.1021/acsenergylett.0c01244.

[59] G. Zhou, Z. Guo, Y. Shan, S. Wu, J. Zhang, K. Yan, L. Liu, P.K. Chu, X. Wu, High-efficiency hydrogen evolution from seawater using hetero-structured T/Td phase ReS₂ nanosheets with cationic vacancies, Nanomater. Energy 55 (2019) 42−48, https://doi.org/10.1016/j.nanoen.2018.10.047.

[60] W. Zang, T. Sun, T. Yang, S. Xi, M. Waqar, Z. Kou, Z. Lyu, Y.P. Feng, J. Wang, S.J. Pennycook, Efficient hydrogen evolution of oxidized Ni-N₃ defective sites for alkaline freshwater and seawater electrolysis, Adv. Mater. 33 (2021) 2003846, https://doi.org/10.1002/adma.202003846.

[61] A.R. Jadhav, A. Kumar, J. Lee, T. Yang, S. Na, J. Lee, Y. Luo, X. Liu, Y. Hwang, Y. Liu, H. Lee, Stable complete seawater electrolysis by using interfacial chloride ion blocking layer on catalyst surface, J. Mater. Chem. 8 (2020) 24501−24514, https://doi.org/10.1039/D0TA08543J.

[62] H. Abe, A. Murakami, S. Tsunekawa, T. Okada, T. Wakabayashi, M. Yoshida, M. Nakayama, Selective catalyst for oxygen evolution in neutral brine electrolysis: an oxygen-deficient manganese oxide film, ACS Catal. 11 (2021) 6390−6397, https://doi.org/10.1021/acscatal.0c05496.

[63] T. Okada, H. Abe, A. Murakami, T. Shimizu, K. Fujii, T. Wakabayashi, M. Nakayama, A bilayer structure composed of Mg|Co-MnO₂ deposited on a Co(OH)₂ film to realize selective oxygen evolution from chloride-containing water, Langmuir 36 (2020) 5227−5235, https://doi.org/10.1021/acs.langmuir.0c00547.